*J. Fluid Mech.* (1982), *vol.* 115, *pp.* 443–451
*Printed in Great Britain*



# The deformation and breakup of a slender drop in an extensional flow: inertial effects

By J. F. BRADY† AND A. ACRIVOS
Department of Chemical Engineering, Stanford University, Stanford, CA 94305

(Received 4 March 1981)

The analysis of Acrivos & Lo (1978) for the deformation and breakup of a slender drop placed symmetrically in an axisymmetric pure straining flow is extended to include the effects of the fluid inertia within the drop. It is shown that, although the flow pattern within the drop is very complicated, internal inertia always tends to stabilize the drop. This stabilizing effect is, however, so weak that, for all practical purposes, it can be ignored.

## 1. Introduction

Since the early experiments of G. I. Taylor (1934), it has been known that drops whose viscosity is much lower than that of the suspending medium become long and slender when subjected to high shear rates and that, if the shear rate is made large enough, the drops will break (Grace 1971; Torza, Cox & Mason 1972; Yu 1974). Taylor (1964) was the first to exploit the drop's slenderness in order to describe theoretically its deformation and breakup. He studied slender drops in an axisymmetric straining motion under conditions of creeping flow and predicted that a drop would break if a critical shear rate were exceeded; specifically, if $(E\mu a/\gamma)\,\lambda^{\frac{2}{3}} > 0{\cdot}148$, where $E$ is the shear rate, $\frac{4}{3}\pi a^3$ is the volume of the drop, $\lambda \equiv \mu_i/\mu$ ($\lambda \ll 1$ for slender drops), $\mu_i$ and $\mu$ are the viscosities of the drop and of the suspending fluid respectively, and $\gamma$ is the coefficient of interfacial tension. More recently, Buckmaster (1972, 1973) and Acrivos & Lo (1978) presented a mathematically systematic development of this slender-body approach and confirmed Taylor's findings. Acrivos & Lo (1978) were also able to incorporate in their analysis the effects of inertia in the suspending fluid, but retained the assumption of zero Reynolds number inside the drop. In addition, Hinch & Acrivos (1979) extended the results of Acrivos & Lo (1978) to the case of a drop placed in a hyperbolic flow – the experimentally used flow field – and showed that, although the drop cross-section is no longer circular, the criterion for breakup is virtually identical with that given by Taylor (the critical value of $E\mu a\lambda^{\frac{2}{3}}/\gamma$ being 0·145 as opposed to 0·148). Hence the theoretical predictions for axisymmetric flow can be compared with experiment, and the agreement is very satisfactory (see Hinch & Acrivos 1979).

All these analyses, which provide a very complete picture of the mechanisms governing the breakup of slender drops, have assumed that the Reynolds number for

† Present address: Department of Chemical Engineering, Massachusetts Institute of Technology, Cambridge, Massachusetts 02139.

the motion inside the drop was small and that the corresponding inertial effects could be neglected. In view of the low values of $\mu_i$, however, in some of the experiments on slender drops, for example those of Taylor (1934), the calculated Reynolds numbers $\rho_i Ea^2/\mu_i$ based on the fluid properties within the drop, with $\rho_i$ being the drop's density, were of order unity or larger at the point of breakup, and hence it seems worth while to extend the theory and to assess the effects of the inertia inside the drop on its dynamics.

We begin with the equation for the shape of the drop, placed symmetrically in an extensional flow, as derived by Acrivos & Lo (1978):

$$\frac{\partial R}{\partial t}+x\frac{\partial R}{\partial x}=-\frac{1}{2G}+\{\tfrac{1}{4}GAx^2+\tfrac{1}{2}p_i\}R, \tag{1.1}$$

$$R(\pm L(t),t)=0, \tag{1.2}$$

where $R(x,t)$ is the distance of any point on the drop's surface from the axis of symmetry scaled with $a\lambda^{\frac{1}{6}}$, $x$ is the distance along this axis and $L$ the half-length of the drop (both scaled with $a\lambda^{-\frac{1}{3}}$), $t$ is the time scaled with $E^{-1}$, and $p_i$ is the pressure within the drop scaled with $\mu E$. Also, $G\equiv E\mu a\lambda^{\frac{1}{6}}/\gamma$ is the appropriate dimensionless shear rate, $A\equiv \rho a\gamma/\mu^2\lambda^{\frac{5}{6}}$ is an inertial parameter which depends only on the physical properties of the external fluid and on the volume of the drop, and their product $GA\equiv \rho Ea^2/\mu\lambda^{\frac{2}{3}}$ is simply the external Reynolds number with the drop's half-length as the characteristic length. Equation (1.1) is correct to leading order in the slenderness ratio with the neglected terms being $O(\lambda)$ and $O(\lambda GA)$. This shape equation is, however, correct for any value of the internal Reynolds number since the latter only affects the internal pressure $p_i$. Aside from a change in notation, (1.1) differs from (5.1) of Acrivos & Lo (1978) in that it includes a time derivative $\partial R/\partial t$ and also leaves the internal pressure $p_i$ unspecified. At zero internal Reynolds number the latter becomes

$$p_i=p_0+8\int_0^x\frac{\xi\,d\xi}{R^2}, \tag{1.3}$$

with $p_0$ an unknown constant, which when substituted in (1.1) gives, at steady state, equation (5.1) of Acrivos & Lo (1978).

In addition to (1.2), which simply requires that the drop close at $x=\pm L(t)$, the solution to (1.1) must satisfy the volume-conservation requirement

$$\int_0^{L(t)}R^2(x,t)\,dx=\tfrac{2}{3}, \tag{1.4}$$

which serves to determine the unknown constant $p_0$ appearing in the expression for the internal pressure $p_i$.

We turn next to computing the critical value of $G$ beyond which a steady drop shape cannot exist.

## 2. The motion within the drop

To assess the effects of internal inertia on the drop's dynamics, we need to determine the pressure distribution inside the drop as a function of the internal Reynolds number, which requires that we examine the motion inside the drop. On using the same non-dimensionalization as before and defining a new radial co-ordinate $r'=r/R(x,t)$

it is easy to show that the equations of motion inside the drop become, to leading order in $\lambda$ (cf. Acrivos & Lo 1978, § 3),

$$GA\eta R^2\left\{\frac{\partial u}{\partial t}+u\frac{\partial u}{\partial x}+\left(v-r'\frac{\partial R}{\partial x}u-r'\frac{\partial R}{\partial t}\right)\frac{1}{R}\frac{\partial u}{\partial r'}\right\}+R^2\frac{dp_i}{dx}=\frac{1}{r'}\frac{\partial}{\partial r'}\left(r'\frac{\partial u}{\partial r'}\right), \tag{2.1}$$

$$\frac{1}{r'}\frac{\partial}{\partial r'}r'v+R\frac{\partial u}{\partial x}-r'\frac{\partial R}{\partial x}\frac{\partial u}{\partial r'}=0, \tag{2.2}$$

with $\eta \equiv \rho_i/\rho$ being the density ratio, and $\partial p_i/\partial r' = O(\lambda)$. We see that (2.1) and (2.2) are types of boundary-layer equations in which the transverse co-ordinate $r'$ is $O(1)$. The motion inside the drop must satisfy a symmetry condition on the axis and lead to a velocity that is continuous across the surface. Thus the boundary conditions for (2.1) and (2.2) are

$$u = x, \quad v = x\frac{\partial R}{\partial x}+\frac{\partial R}{\partial t} \quad \text{at} \quad r' = 1, \tag{2.3a,b}$$

$$\frac{\partial u}{\partial r'} = v = 0 \quad \text{at} \quad r' = 0. \tag{2.4a,b}$$

Also, $u$ must be odd in $x$.

In addition to the drop shape and length, the only parameter of the system that describes the internal motion is the internal Reynolds number

$$GA\eta R^2 = \left(\frac{\rho_i E a^2}{\mu_i}\lambda^{\frac{1}{3}}\right)R^2(x,t),$$

which is simply a Reynolds number expressed in terms of the local radius and the properties of the fluid within the drop. The appearance of the local radius as the characteristic length scale is appropriate because the motion corresponds to that for the flow in a long slender tube of slowly varying cross-section. We also see that the previous analyses for zero internal inertia refer to $\eta \equiv 0$, in which case it is easy to show that $R^2 dp_i/dx = 8x$, and that (1.3) is recovered for the steady internal-pressure distribution. Hence, strictly speaking, the previous analyses are only valid when $\rho_i/\rho \ll 1$, while most of the relevant experimental results are for $\eta \simeq 1$.

Rather than attempt to solve the full, coupled problem – (1.1), (1.2) and (1.4) for the shape and (2.1)–(2.4) for $p_i$ – we shall first invoke a simple approximation similar to that employed by Acrivos & Lo (1978) in their analysis (cf. their § 5). Specifically, we represent the drop shape by the quadratic expression

$$R(x) = \frac{1}{2}\left(\frac{5}{L}\right)^{\frac{1}{2}}\left\{1-\frac{x^2}{L^2}\right\}, \tag{2.5}$$

which satisfies (1.2) and (1.4), and approximate the internal pressure by

$$p_i = p_0+\tfrac{1}{2}\beta x^2. \tag{2.6}$$

As will be seen below, the coefficient $\beta$ can be determined as a function of the internal Reynolds number, i.e. as a function of $GA\eta$, and hence, combining (2.5) and (2.6) with (1.1), we obtain a relation between $L$ and the parameters $G$, $A$ and $\eta$. As shown by Acrivos & Lo (1978), when the internal inertia is zero, this approximation gives critical shear rates at breakup that are within 1–2 % of the exact values over the entire range of $A$; in fact the critical shear rate thereby calculated agrees with the exact result when $A = 0$. Thus this approximation offers the possibility of assessing the effects of internal inertia by means of a very simple method.

We next seek an approximate steady-state solution to the appropriate equations, by expanding the velocity field in the form

$$u = x\frac{f'(r)}{r} + O(x^3), \quad v = -\frac{f(r)}{r} + O(x^2), \tag{2.7a,b}$$

which, when substituted, together with (2.5) and (2.6), into (2.1)–(2.4), yields, on balancing the $O(x)$ terms, a third-order ordinary differential equation for $f$ with four boundary conditions, the fourth serving to determine the pressure coefficient $\beta$. In fact, this ordinary differential equation for $f$ represents an exact similarity solution to the full time-independent Navier–Stokes equations for the steady flow in a semi-infinite tube, which was considered in detail in a separate publication, Brady & Acrivos (1981), where it was shown that the solution (2.7) has the remarkable property that it ceases to exist within the internal-Reynolds-number range $10{\cdot}25 < GA\eta R^2 < 147$ (see figure 7 in Brady & Acrivos 1981).

At first glance, the non-existence of similarity solutions for values of the internal Reynolds number beyond 10·25 is puzzling because this parameter actually decreases with increasing shear rate. This is because the length of the drop grows at least as rapidly at $G^2$ – cf. equation (3.12) of Acrivos & Lo (1978) – and thus, since the internal Reynolds number is based on the drop radius, this Reynolds number decreases more rapidly than $G^{-1}$. The significance of the similarity solution is therefore open to question because it would appear that, in a typical experiment involving a gradual increase in the shear rate, a state in which the internal Reynolds number equals 10·25 could only be reached from states of higher Reynolds numbers where steady solutions to the similarity equation do not exist.

The determination of the motion inside the drop when $GA\eta R^2 > 10{\cdot}25$ and the resolution of the paradox regarding the non-existence of similarity solutions within a certain Reynolds-number range have been discussed elsewhere, Brady & Acrivos (1982), and hence we shall only briefly outline the results.

By supposing that the longitudinal velocity can be expanded in a Taylor series about the origin, we have implicitly assumed that the fluid that is returning from the end of the drop exerts no influence on the motion near $x = 0$. Specifically, the similarity solution (2.7) requires that the axial velocity of the returning fluid vanish as $x \to 0$, which can only happen if the internal Reynolds number is sufficiently small. On the other hand, when this Reynolds number is large, the viscous forces, which play the dominant role in slowing down the returning fluid, are too weak to overcome the momentum of this fluid by the time the latter has reached the origin. Hence, once the critical Reynolds number of 10·25 is exceeded, the returning fluid 'collides' with its mirror image from negative $x$, forming, as we have shown (Brady & Acrivos 1982), an inviscid region of flow near $x = 0$, termed the collision region, in which the similarity solution no longer applies.

From a mathematical point of view, (2.1) is not valid in an $O(\lambda^{\frac{1}{3}})$ region of $x = 0$, because when the axial co-ordinate is small it should be scaled in exactly the same way as the radial co-ordinate, i.e. with $a\lambda^{\frac{1}{3}}$ rather than with $a\lambda^{-\frac{1}{3}}$. Thus, (2.1) should be viewed as applying to the flow in an 'outer' region whose solution must match with the solution to an equation valid in an 'inner' region near $x = 0$. The problem of determining the motion inside the drop is then equivalent to that of selecting the initial condition for the boundary-layer equation (2.1) that properly takes into account

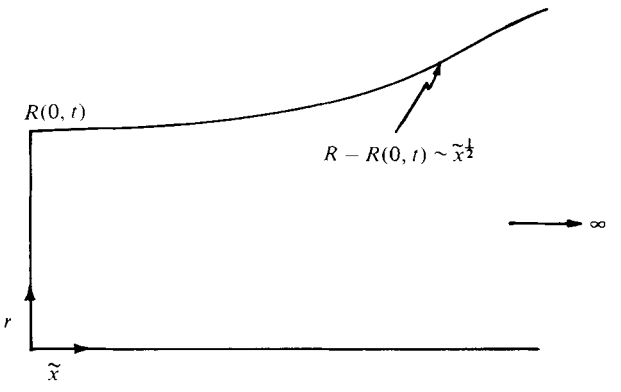


FIGURE 1. Schematic diagram indicating the shape of the drop within the inviscid collision region near $x = 0$. The drop surface must have a minimum at $\tilde{x} = 0$ and grow as $\tilde{x}^{\frac{1}{2}}$ as $\tilde{x} \to \infty$, where $\tilde{x}$ is the axial co-ordinate non-dimensionalized with $a\lambda^{\frac{1}{6}}$.

the presence of the reverse flow. A scheme for accomplishing this was presented by Brady & Acrivos (1982), who also obtained numerical solutions to (2.1)–(2.4) (for a given $R(x,t)$) up to Reynolds numbers $O(10^2)$. Since, in the present case, $R(x,t)$ is *a priori* unknown, the shape equation (1.1) and the equations of motion within the drop must be solved together dynamically in time in order to model properly the drop's deformation and the conditions for breakup.

The flow inside the drop was determined by using the same numerical, finite-difference scheme developed in Brady & Acrivos (1982). Equations (2.1)–(2.4) were first transformed to a fixed domain by scaling both $x$ and $u$ by $L(t)$, and using $r^2/R^2(x,t)$ as the radial co-ordinate. This eliminated all of the time-dependent terms from the boundary conditions and maintained the computational grid fixed as the drop shape evolved in time. Rather than solving the complete time-dependent equation, however, the terms resulting from this transformation which contained $\partial R/\partial t$ and $dL/dt$ were set equal to zero because this enhanced the stability of the numerical scheme and permitted the use of a larger time step, thus saving computing time. Hence, (2.1) was solved at each time step as if the shape $R$ and the length $L$ were fixed, but, of course, both were changed from one time step to the next via the shape equation (1.1) (see below). Although this approximation is not dynamically correct, it does not affect the steady solutions nor did it significantly affect the time evolution of the shape. In general, the changes in the shear rate $G$ and the time-step size, particularly near the critical shear rate, were such that both $\partial \ln R/\partial t$ and $d \ln L/dt$ were typically small.

As we have shown (Brady & Acrivos 1982), when the internal Reynolds number exceeds 10·25 and a collision region is present at $x = 0$, the pressure $p_i$ in (2.1) will be linear in $x^{\frac{1}{2}}$ as $x \to 0$, which implies from (1.1) that $R$ should likewise be linear in $x^{\frac{1}{2}}$ for small $x$. Furthermore, the pressure within the $O(\lambda^{\frac{1}{3}})$ thick collision region will vary by an $O(1)$ amount, which will cause the drop's surface to deform. Noting that $x = 0$, $r = R(0,t)$ is a stagnation point of the flow, it follows from Bernoulli's equation that the internal pressure will have a maximum at this point. This in turn implies that the radius will have a local minimum at $x = 0$, and therefore the drop surface within the collision region should have the shape illustrated in figure 1.

Since the variation in the shape is $O(1)$ within the collision region, it is virtually impossible to carry out an analysis of how the surface deforms. We must, therefore,

assume that, within the collision region, the surface tension is able to balance the pressure variation for all $G$ (the flow outside the drop being essentially stagnant), and that the fluid motion in this region does not affect the drop's dynamics. These assumptions are based on the fact that two destabilizing forces are needed to break a drop, and that it is the overall length $L$, not any local region of the surface, which is important in determining the deformation and breakup. Moreover, the small fraction of the drop's length within which the pressure is proportional to $x^{\frac{1}{2}}$ is really part of the collision region, and it appears logical to assume that this small region will not exert any significant effect on the drop's dynamics. Accordingly, we shall not require that the shape $R$ be linear in $x^{\frac{1}{2}}$ for small $x$ (see below). Similarly, it will not be necessary to solve (2.1) with sufficient accuracy to resolve the square-root dependence of $p_i$ at $x = 0$, which allows us to use a very coarse finite-difference mesh, thereby rendering the computations tractable in a finite amount of computing time. Thus, although the collision region is needed in order for solutions to exist for the flow inside a drop when the internal Reynolds number exceeds 10·25, we shall assume that it plays no direct role in determining the conditions for breakup.

The numerical solution for the motion inside the drop can easily be computed using a finite-difference scheme, but greater care is needed in solving the shape equation. As we have seen, the zero-internal-Reynolds-number solution for the internal pressure, (1.3), indicates that the pressure is singular at the tip, i.e. $p_i \sim 1/R$ as $x \to L$. However, the surface-tension force is also proportional to $1/R$, and hence these two forces balance exactly at the tip. This singularity can cause difficulties if a finite-difference scheme is used to compute the shape, and thus we have chosen to solve the shape equation by means of modal functions. This idea of approximating the shape as a series of modal functions whose coefficients depend on time was used very successfully by Hinch & Acrivos (1980) when studying a slender viscous drop in a simple shear flow. For modal functions we shall employ simple polynomials and express $R(x, t)$ as a power series in $x$ of degree $N$ with coefficients that depend on time, i.e.

$$R(x,t) = \sum_{n=0}^{N} a_n(t)\,|x|^n. \tag{2.8}$$

When a collision region is present, odd powers of $x$ are needed because the shape is no longer simply a function of $x^2$.

In using this polynomial approximation for the shape, we must also approximate the pressure $p_i$ as a series in $x$; thus, for the pressure we write

$$p_i = p_0(t) + \int_0^x \frac{R^2\, dp_i/d\xi}{R^2}\, d\xi, \tag{2.9}$$

where $p_0(t)$ is the unknown constant value at the origin. The numerical, finite-difference solution of (2.1) gives directly $R^2\, dp_i/dx$ at each grid point, and through this discrete set of points a polynomial can be fitted. The degree of this polynomial was selected so as to minimize the standard deviation of the computed $R^2\, dp_i/dx$ from their approximated values, which normally resulted in a polynomial of degree 6. The numerator and denominator of (2.9) were then expanded, integrated and the resulting sum truncated to $N$ terms. Upon substituting (2.8) and the resulting expansion for (2.9) into the shape equation (1.1), we develop a system of $N$ coupled equations for the time rate of change of the coefficients $a_n(t)$.

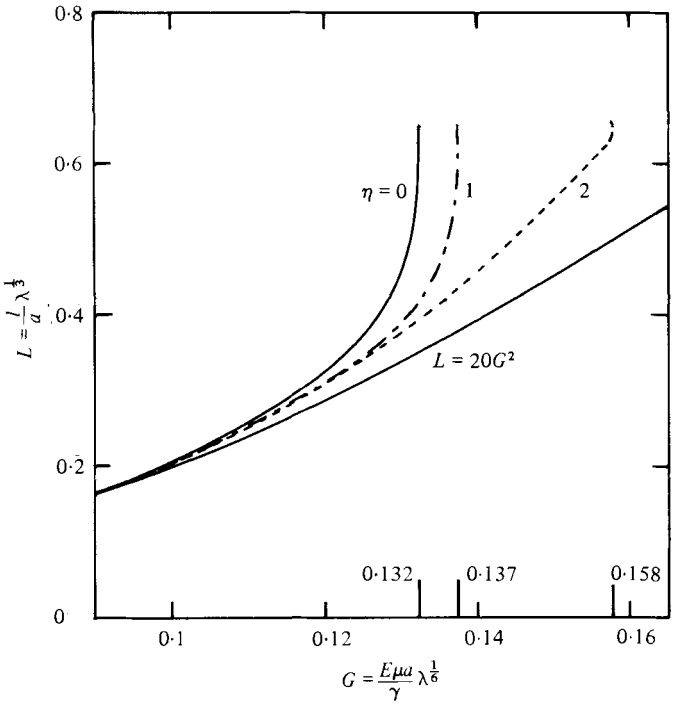


FIGURE 2. Steady dimensionless drop length as a function of the dimensionless shear rate for $A = 25$ from the solution of the shape equation (1.1): ——, $\eta = 0$; — – —, $\eta = 1$; ---, $\eta = 2$. (Solid curve $L = 20G^2$ corresponds to a bubble in a purely viscous flow.)

The pressure $p_0(t)$ must be found from the volume-conservation relation (1.4), and this can be easily implemented by noting that $R_t$ is linear in $p_0(t)$, and that

$$\int_0^{L(t)} RR_t\,dx = 0, \tag{2.10}$$

which follows upon differentiating the volume-conservation relation. Thus we can solve (1.1) for $R_t$ for two arbitrary values of $p_0$, and then take the linear combination which satisfies (2.10). In performing the integration in (2.10), $RR_t$ must not be truncated to $N$ terms, but the full $2N-1$ terms kept in order to avoid losing fluid. The fact that the volume is conserved, or almost conserved, throughout many time steps provides a very good check on the numerical method. Over time, however, some slight drift in the volume of the drop was encountered, which is equivalent to changing $G$; therefore the shape was periodically renormalized in order to insure that the volume was conserved.

The equilibrium drop length and shape for given set of values of the physical parameters $G$, $A$ and $\eta$, was determined as follows. At $t = 0$ the flow field inside the drop and the drop shape were set equal to their steady solutions at another set of $G$, $A$ and $\eta$. Using the linearity in $p_0(t)$, $R_t$ was calculated from (1.1) and the new shape computed at one time step later. The new drop length was then found by locating the nearest zero of the polynomial (2.8) by Newton's method. With this new shape and length, the flow field and pressure distribution within the drop were recalculated at the next time step using the numerical scheme described by Brady & Acrivos (1982), and thus a new

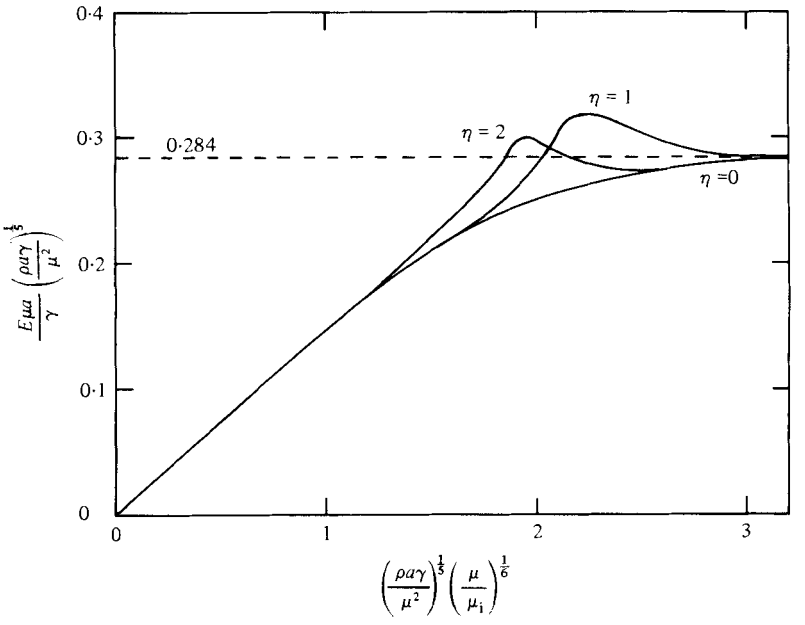


FIGURE 3. Critical shear rates at breakup, $GA^{\frac{1}{3}}$, from the complete solution of both the shape equation and the motion within the drop, as functions of the inertial parameter $A$ for $\eta = 0, 1, 2$.

$R_t$ could be computed from (1.1). The procedure was then repeated until a steady solution was reached for the shape, the length and the flow field within the drop.

The critical shear rate at breakup as a function of $A$ and $\eta$ was found by repeating the above calculations for successively large values of $G$ until a steady solution could no longer be attained. This entire process had to be repeated for various values of the two parameters $A$ and $\eta$, which obviously would have required an enormous amount of computing. Hence, the critical conditions at breakup were only determined for two values of the density ratio, $\eta = 1$ and $\eta = 2$, which cover the range of greatest practical interest. Indeed, it is very difficult to find a combination of fluids for which the fluid of very high density ($\eta \gg 1$) also has a very low viscosity ($\lambda \ll 1$).

Normally 12 terms were used in the polynomial approximation for the shape, although some solutions were constructed with as few as 4 and as many as 20 and gave drop shapes, lengths and critical shear rates which were within 1–2 % of those obtained with the 12-term expansion. Most of the computational time was consumed in calculating the flow inside the drop; thus, a coarse $11 \times 21$ (axial $\times$ radial), finite-difference grid was found to be optimal in terms of the trade-off between accuracy and computing time. Spot checks with finer computational grids were made periodically, and the overall accuracy of the numerical calculations was estimated to be approximately 3 %.

Figure 2 shows the deformation relation, i.e. $L$ versus $G$, for three values of $\eta$ at $A = 25$. We see that the effects of internal inertia are to stabilize the drop – that is, larger shear rates at breakup are required when the internal inertia is non-zero – but that the effect is weak. Figure 3 shows the complete calculations for the critical shear rate at breakup as a function of $A$ and $\eta$. The curve corresponding to $\eta = 0$ represents the results of Acrivos & Lo (1978) for zero internal inertia. $GA^{\frac{1}{3}}$ has been plotted versus $A$ because, for the case of an inertialess bubble ($\eta = 0, \lambda = 0$) in an inertial extensional

flow ($A \neq 0$), the equations should be rescaled so as to eliminate $\lambda$, and $GA^{\frac{1}{5}}$ is then the appropriately non-dimensional shear rate. At low values of $A$, the inertial effects both inside and outside the drop are small, and the drop behaves as if it were purely viscous and suspended in a zero-Reynolds-number flow. Thus the critical shear rate at breakup approaches 0·148 as $A \to 0$. At the other extreme, when $A$ is large, the inertia of the exterior fluid dominates, and the drop breaks when $GA^{\frac{1}{5}}$ exceeds 0·284. It is only in the intermediate range of $A$ that the inertial flow inside is able to partly counterbalance the stresses due to the inertia outside and slightly stabilize the drop.

Thus, we have been able to determine the deformation and critical conditions at breakup when the internal inertia is non-zero. The relatively weak effect of the internal inertia implies that one *can* use the zero-internal-inertia results to predict drop breakup, and it also helps to explain why the previous theories, which neglect internal inertia, are in good agreement with experiment. For density ratios less than 2, the error will be at most 20 %, which is not very large considering the inherent difficulty in performing the experiments.

This work was supported in part by the National Science Foundation under grant ENG-78-17613 and by N.A.T.O. research grant 1442.

## REFERENCES

ACRIVOS, A. & LO, T. S. 1978 The deformation and breakup of a single slender drop in an extensional flow. *J. Fluid Mech.* **86**, 641–672.

BRADY, J. F. & ACRIVOS, A. 1981 Steady flow in a channel or tube with an accelerating surface velocity. An exact solution to the Navier–Stokes equations with reverse flow. *J. Fluid Mech.* **112**, 127–150.

BRADY, J. F. & ACRIVOS, A. 1982 Closed-cavity laminar flows at moderate Reynolds numbers. *J. Fluid Mech.* **115**, 427–442.

BUCKMASTER, J. D. 1972 Pointed bubbles in slow viscous flow. *J. Fluid Mech.* **55**, 385–400.

BUCKMASTER, J. D. 1973 The bursting of pointed drops in slow viscous flow. *Trans. A.S.M.E.* E, *J. Appl. Mech.* **40**, 18–24.

GRACE, H. P. 1971 Dispersion phenomena in high viscosity immiscible fluid systems and applications of static mixers as dispersion devices in such systems. *Engng Found. 3rd Res. Conf. Mixing, Andover, New Hampshire.*

HINCH, E. J. & ACRIVOS, A. 1979 Steady long slender droplets in two-dimensional straining motion. *J. Fluid Mech.* **91**, 401–414.

HINCH, E. J. & ACRIVOS, A. 1980 Long slender drops in a simple shear flow. *J. Fluid Mech.* **98**, 305–328.

TAYLOR, G. I. 1934 The formation of emulsions in definable fields of flow. *Proc. R. Soc. Lond.* A **146**, 501–523.

TAYLOR, G. I. 1964 Conical free surfaces and fluid interfaces. In *Proc. 11th Int. Cong. Appl. Mech., Munich*, 1964 (ed. H. Görtler), pp. 790–796. Springer.

TORZA, S., COX, R. G. & MASON, S. G. 1972 Particle motions in sheared suspensions. XXVII. Transient and steady deformation and burst of liquid drops. *J. Colloid Interface Sci.* **38**, 395–411.

YU, K. L. 1974 Ph.D. thesis, University of Houston.